# Primary insights into the superconducting twin qubit


I. V. Antonov

*Royal Holloway, University of London, Egham, TW20 0EX, UK and National Physical Laboratory, Hampton Road Teddington, TW11 0LW, UK*

R. S. Shaikhaidarov

*Royal Holloway, University of London, Egham, TW20 0EX, UK*

V. N. Antonov

*Royal Holloway, University of London, Egham, TW20 0EX, UK Skolkovo Institute of Science and Technology, Nobel str. 3, Moscow, 143026, Russia and Moscow Institute of Physics and Technology, 29 Institutskiy per., 141700 Dolgoprudny, Moscow Region, Russia*

O.V. Astafiev

*Royal Holloway, University of London, Egham, TW20 0EX, UK Skolkovo Institute of Science and Technology, Nobel str. 3, Moscow, 143026, Russia and National Physical Laboratory, Hampton Road Teddington, TW11 0LW, UK*



(Dated: July 3, 2019)



A platform of quantum computation based on superconducting qubits is at the frontiers of realization, owing to the scalability and breadth of implementation by modern nanofabrication technology. However the simplicity and flexibility of fabricating superconducting qubits compared with other qubit architectures has to be set against their limited ability of handling only limited sequential state operations. The most successful processor prototype has a decoherence time of $\sim 60\,\mu$s while the gate operation time is about $20\,\mu$s. Therefore, within 3 gate operations it's quantum state becomes substantially deteriorated. Thus short decoherence time stands as one of the obstacles hinderinglarge scale implementation of superconducting quantum processors.

In this work we look at a new "twin-qubit" geometry - a fusion of two flux qubits joined by a common Josephson Junction, which can potentially outperform current devices. At the degeneracy flux-bias point, $\Phi_0/2$, the twin qubit has energy spectrum plateaus with curvature several orders of magnitude lower than that in the usual flux qubits. This flatness makes the qubit more robust to flux noise. Also, the new qubit allows the $|1\rangle \leftrightarrow |2\rangle$ dipole transition at the aforementioned degeneracy point, where coherence time is longest. This transition is forbidden in other qubit designs. We experimentally study the new qubit, get the transmission spectrum, Rabi oscillations, and fully simulate the operation of the qubit. Potentially the new qubit may outperform the conventional flux qubit designs.


## I. INTRODUCTION

Superconducting qubits are one of the promising trends for implementing quantum computing technology. Typical qubits are on-chip aluminum structures with Josephson junctions (JJ), whose geometry can be designed to select an operating energy, state transition rates and sensitivity required in a particular environment. Over the past decade they have carried out the functionality of a transistor [1, 2], where a control field was used to pass or block a second field at a different frequency, multiplexer [3], two input signals can be mixed to controllably generates a single output signal, and serial bus [4]. Superconducting qubits can be produced using industry standard nanofabrication techniques and integrated at scale into large coherent circuits [5]. All speaks to a strong case of servicing future quantum electronic platforms with this technology.

One of the inherent limitation superconducting qubits face is a comparatively short coherence time, $\tau_{\text{dec}}$, beyond which quantum information becomes lost, (see Appendix A). For example, the transmon qubits in the revolutionary 5-qubit quantum experience from IBM (research.ibm.com/ibm-q) have a coherence time of only $60\,\mu$s [6]. In order to have a sufficient number of quantum logic operations for multi-stage computations, say $10^4$, coherence times need to surpass the $100\,\mu$s barrier.

Strong decoherence in superconducting qubits is partially a consequence of the large capacitances inherent to their geometry. The superconducting loops in flux qubits are typically $1\,\mu$m or greater in size [2, 5], which couples them to charge variations in the external environment. Such fluctuations modify the qubit's energy levels, consequently leading to an erratic evolution of the quantum state which 'washes' out quantum information [9].

Particularly in flux qubit architectures the JJ energy dominates over the charging energy, $E_J/E_C >> 1$, which lowers the device's charge sensitivity [8, 10, 11]. A whole family of flux qubit designs have lead to improvement of the coherence times: shunted flux qubit $\sim 80\,\mu$s [15] , 4-JJ qubit [16], fluxonium $\sim 1$ ms [17].

Here we investigate experimentally a 'twin' qubit, consisting of two symmetrical flux qubits, linked by a common $\alpha-$Josephson Junction (Fig. 1). A chain of 15 such qubits was recently placed into a coplanar waveguide to demonstrate flux-tunable transmission of microwaves [18]. Of particular interest to us is the weak flux dependence of the systems transition energy when it was biased to the degeneracy point $\Phi_0/2$, making it benefit from both low flux and charge sensitivities.

In this work we characterize the twin qubit in a way that has not been done before - we isolate one of the qubits and realize it's capacitive coupling to the transmission line. We provide the first experimentally measured transmission spectrum and find: strong anharmonicity with respect to the $|1\rangle \leftrightarrow |2\rangle$ and $|2\rangle \leftrightarrow |3\rangle$ transitions; weak flux dependence of the transition energies close to the degeneracy point; compliance of the experimental energy spectrum with simulations and outstanding features of the $|1\rangle \leftrightarrow |2\rangle$ dipole transition.

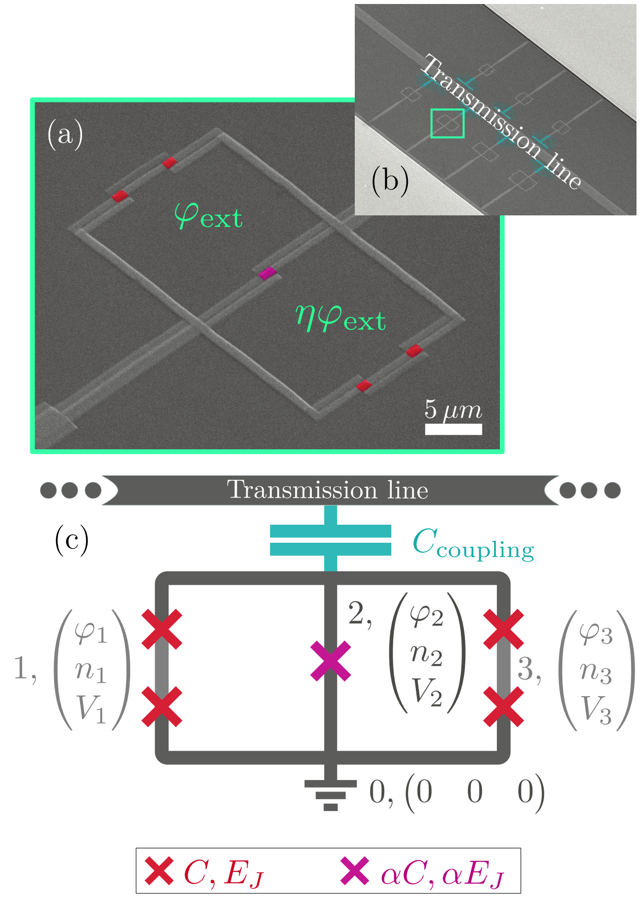


FIG. 1. **Geometry of a twin qubit:** (a) Scanning electron microscope image of the twin qubit. The Al-AlO$_x$-Al JJs are highlighted in red and pink; (b) Each of the qubits is coupled to the transmission line with a T-shaped capacitor; (c) The twin qubit is a symmetrical arrangement of two individual flux qubits (as described in [8]) sharing the central JJ. Islands are labeled with a Cooper pair occupation $n_i$, phase $\varphi_i$ and voltage $V_i$, with the ground setting a reference of 0 for all three variables. JJs (marked with crosses) mediate capacitive and Josephson interactions between the islands.

## II. SAMPLE DETAILS

The sample is fabricated on an undoped 100 silicon substrate, which is pre-patterned with 10 nm NiCr - 90 nm Au ground planes. We use an electron beam lithographer and a shadow evaporation technique to create the structure of Fig. 1. The qubit consits of five JJ junctions integrated into two symmetrical superconducting loops. The JJ have a layered structure of Al (20 nm) - $AlO_x$ (oxidized for 10 min at 0.3 mbar) - Al(30 nm). The energy and capacitance of the central JJ is a factor of $\alpha$ larger than for the outside ones, which have dimensions $400 \times 200\,\text{nm}^2$. The coplanar transmission line with impedance $Z_0 \sim 50\,\Omega$ runs to the opening between the ground planes in the center of the chip. The qubits are capacitively coupled to the transmission line through T-shaped capacitors. Phase biases $\varphi, \eta\varphi$, are applied to the two superconducting loops with an external magnetic field.

We mount our sample on a holder with a superconducting-coil magnet on the 13 mK stage of a dilution refrigerator. A superconducting shield is used to screen the holder from stray magnetic fields. The RF lines connected to the sample have attenuators for thermalization: -50 dBm on the 50K stage, -30 dBm on the 4 K stage. We attach a circulator on the output line for isolation. The transmitted signal is amplified by +35 dBm on the 4K stage and by +35 dBm at room temperature. This set of attenuators and amplifiers facilitate power conversion between the laboratory equipment and qubit microwaves. Prior to performing characterization measurement, we took the microwave transmission spectrum with the qubit detuned, and correct all measurements by the background transmission profile.

Our primary goal in the experiment was to study the intrinsic energy structure of the qubits and compare it with the theory, as opposed to achieving competitive performance. Fabrication did not to go to the depths of chemical and physical treatment of the substrate surface to remove two-level system defects in the silicon oxide layer [20] and we did not employ infra-red filters to eliminate stray light during measurement [21]. There steps would nevertheless be necessary if one is to improve the parameters of the qubit.

## III. OPERATIONS WITH QUBITS

We record the energy spectrum of the twin qubit using a network analyzer, while sweeping the biasing magnetic flux. Because of a small asymmetry, $\eta$, the fluxes linked through the left and right loops are slightly different: $\Phi = \frac{\varphi}{2\pi}\Phi_0$ and $\eta\Phi$, where $\eta \approx 1$.

The $|1\rangle \leftrightarrow |2\rangle$ transition, $\omega_{21}$, is mapped with a network analyzer which measures the transmission of signal $\omega_{\mathrm{NA}}$ through the system. Away from resonance the signal passes through the circuit without any interaction with the qubit. After correcting for the line losses, transmission is close to 100%. Only near resonance ($\omega_{\mathrm{NA}} = \omega_{21}$), does the qubit exchange photons with the driving field as it evolves between the ground and excited states. The qubit emits a wave that is exactly in anti-phase with the driving field [22], and the destructive superposition in the output line results in a transmission dip, see Fig. 2. The trace of blue circles of the transmission minima at different magnetic flux maps out the qubit's $\omega_{21}$ transition spectrum, see inset of Fig. 2.

The $|2\rangle \leftrightarrow |3\rangle$ transition, $\omega_{32}$, is mapped using two-tone spectroscopy. The network analyzer probes signals at $\omega_{21}$, while an additional generator sweeps a second frequency, $\omega_{\mathrm{GEN}}$. Whenever the generator strikes the $|2\rangle \rightarrow |3\rangle$ transition ($\omega_{\mathrm{GEN}} = \omega_{32}$), the qubit undergoes a ladder of excitations, $|1\rangle \xrightarrow{\omega_{21}} |2\rangle \xrightarrow{\omega_{32}} |3\rangle$, depopulating states $|1\rangle$ and $|2\rangle$. Because of this depopulation, the probe signal is no longer absorbed to drive the $|1\rangle \leftrightarrow |2\rangle$ transmission, and it's transmission moves out of the resonance dip in Fig. 2. This identifies $\omega_{32}$ which is mapped with red circles in the transition energy-magnetic field spectrum.

We match the experimental data points to simulations: Islands, isolated by the JJ in Fig. 1, are labeled with Cooper pair (CP) occupation $\vec{n} = |n_1, n_2, n_3\rangle$, phase $\vec{\varphi} = |\varphi_1, \varphi_2, \varphi_3\rangle$ and potential $\vec{V} = |V_1, V_2, V_3\rangle$ states. The charges and potentials on the islands are

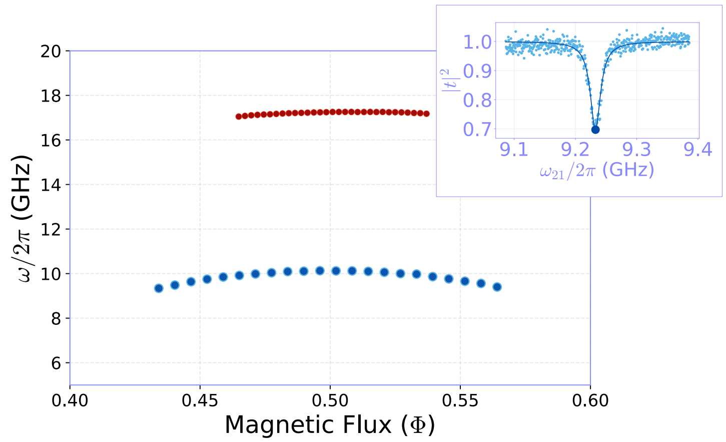


FIG. 2. **Mapping the qubit transition spectrum:** For the lower transition $\omega_{21}$ (blue) a network analyzer measures the power transmission coefficient, $|t|^2$, at flux bias $\Phi$ and microwave frequency $\omega_{21}/2\pi$. A Lorentzian fit [1] to the transmission profile establishes the resonant frequency, which is marked with blue points on the flux-frequency spectrum. For transition $\omega_{32}$ (red) a two-tone measurement is run by monitoring changes to a weak $\omega_{21}$ probe while sweeping a second frequency in search of the higher transition.

linked by the capacitance matrix

$$2e\vec{n} = \hat{C}\vec{V}.$$

The capacitance matrix in the twin qubit topology is

$$\hat{C} = |C| \begin{pmatrix} 2 & -1 & 0 \\ -1 & 2+\alpha & -1 \\ 0 & -1 & 2 \end{pmatrix},$$

where $|C|$ is the capacitance of the outer JJs. The interaction of the CPs, carrying a charge $\vec{Q} = 2e\vec{n}$, and potentials on their respective islands gives rise to the 'kinetic' term of the Hamiltonian:

$$T = \frac{1}{2}\sum_{i=1}^{3} Q_i V_i = \frac{(2e)^2}{2}\vec{n}\hat{C}^{-1}\vec{n}^T$$
$$= E_C\,|C|\left\langle \hat{C}^{-1}\right\rangle_{|n_1,n_2,n_3\rangle},$$

where we define $E_C = (2e)^2/2\,|C|$.

Each JJ with a phase difference of $\Delta\varphi_i$, contributes an energy of $E_{Ji}\,(1 - \cos(\Delta\varphi_i))$. The flux quantization condition for the left and right loops, $\sum_i^{\mathrm{loop}} \varphi_i = 2\pi n, n \in \mathbb{Z}$, enters as a dependence on

$\varphi_{\rm ext}$ and $\eta\varphi_{\rm ext}$ on two of the junctions:

$$U = E_J\big[4+\alpha-\alpha\cos(\varphi_2)-\cos(\varphi_1)-\cos(\varphi_3)- \\ \cos(\varphi_2-\varphi_1-\varphi_{\rm ext})-\cos(\varphi_2-\varphi_3+\eta\varphi_{\rm ext})\big].$$

The Hamiltonian, $\mathcal{H} = T + U$, is solved in the charge basis (see Appendix B) with $E_J = 91.0\,$GHz, $E_C = 13.50\,$GHz, $\alpha = 1.023$ , $\eta = 1.011$ . The resulting eigenenergies are compared with the experimental ones in Fig. 3 . Data for $\omega_{32}$ is taken in a narrow flux range because away from $\Phi = n\Phi_0, n \in \mathbb{Z}$, it gets harder to tune the VNA to $\omega_{21}$ in two-tone spectroscopy. The asymmetry value, $\eta$, is close to the visual loop area difference of 3% seen from the SEM image in Fig. 1. The resonance is periodic in flux, with a tendency of higher $\omega_{21}$ at higher magnetic flux numbers.

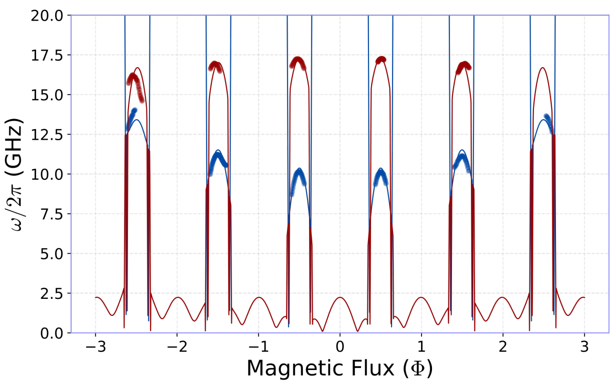


FIG. 3. **Experimental spectra, circles, and simulation, solid lines, of the twin qubit:** Shown are the transition frequencies $\omega_{21}$ (blue) and $\omega_{32}$ (red). Asymmetry in the flux penetrating the left and right loops results in the gradual change of transition frequencies with every $\Phi_0$ period: $\omega_{21}$ creeps up, while $\omega_{32}$ creeps down, breaking the usual periodicity of flux qubits.

An important qubit parameter is the curvature at the turning points in the energy spectrum, at the operation point of the qubit. A low curvature is desirable, to make the qubit less sensitive to external flux changes, which would improve decoherence time. At the twin qubits' degeneracy points $\Phi = n\Phi_0, n \in \mathbb{Z}$, the curvature is $(-550 \pm 10)\,{\rm GHz}/\Phi_0^2$. It is substantially smaller than $13 \times 10^4$ GHz/$\Phi_0^2$ on the 4-JJ flux qubit [14], $8.4 \times 10^4\,{\rm GHz}/\Phi_0^2$ [23] and $37 \times 10^4$ GHz/$\Phi_0^2$ [24] on the 3-JJ flux qubits demonstrated recently. However, the decoherence time of $= 42\,$ns, taken with Rabi oscillation [25–27] was relatively short, see Fig. 4. We attribute this to poisoning of the sample with the infrared radiation, and the coupling two-level oscillators in the substrate, owing to the simplified technology used in the qubit's fabrication.

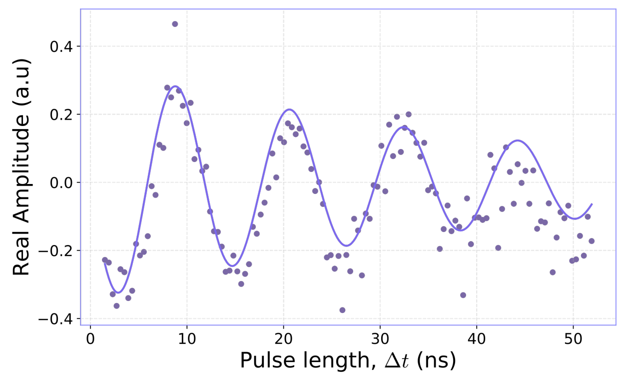


FIG. 4. **Rabi oscillations:** taken at the degeneracy point by driving the qubit with resonant microwaves pulses for fixed time periods, $\Delta t$. The decoherence time of $\tau_{\rm dec} = 42\,$ns is extracted from the decay envelope, $e^{-\Delta t/\tau_{\rm dec}}$, of the the oscillations.

## IV. DIPOLE TRANSITION

Finally we characterize the dipole moment of transition between the lowest two states, $|1\rangle$ and $|2\rangle$. Microwaves in the transmission line, with voltage $V_{\rm mw} = |V_{\rm mw}|\cos(\omega_{21}t)$ are coupled via capacitor $\mathrm{C}_{\rm coupling}$ to the qubit. On island 2 the microwave induces a charge $Q_2 = C_{\rm coupling}V_{\rm mw}$. Transitions $|1\rangle \leftrightarrow |2\rangle$ stimulated by this driving generate a qubit voltage of $\delta V_2 = \langle 1|\,\hat{V}_2\,|2\rangle$ between the ground and island 2 and hence draw an electrostatic energy related to the strength of the drive $\Omega$ by:

$$\delta V_2 Q_2 = \langle 1|\,\hat{V}_2\,|2\rangle\, C_{\rm coupling}\,|V_{\rm mw}|\cos(\omega_{21}t) \\ = \hbar\Omega\cos(\omega_{21}t).$$

Thus, up to the constant of proportionality $Q_2$, evaluation of

$$\delta V_2 = \langle 1|\,\frac{E_C}{2\,|e|\,(1+\alpha)}\,[\hat{n}_1 + 2\hat{n}_2 + \hat{n}_3]\,|2\rangle$$

gives the coupling strength $\Omega$ between the microwave line and the qubit system. To quantitatively compare coupling strength between different flux qubit geometries, we re-write the voltage element using flux:

$$\begin{aligned}\langle 1|\,\hat{V}_2\,|2\rangle &= \frac{d}{dt}\,\langle 1|\,\hat{\Phi}_2\,|2\rangle \\ &= \frac{d}{dt}\left[\left(e^{i\omega_{21}t/2}\,\langle 1|\right)\hat{\Phi}_2\left(e^{+i\omega_{21}t/2}\,|2\rangle\right)\right] \\ &= i\omega_{21}\beta\Phi_0,\end{aligned}$$

In the last equation we use the free evolution of a two-level system, $U(t) = e^{-i\frac{\mathcal{H}}{\hbar}t}$, $\mathcal{H} = -\frac{\hbar\omega_{21}}{2}\sigma_z$, to draw out the time-dependent phases in $\delta V_2$. The dimensionless parameter $\beta = \langle 1|\hat{\Phi_2}|2\rangle/\Phi_0$ is the normalized coupling constant that can be compared across geometries.

In Fig. 5, we compare $\beta$ between the twin qubit and a 4-JJ flux qubit [3] . Irrespective of the energies used in the simulations, the twin qubit always has a local maximum of coupling strength at degeneracy points $\Phi = n\Phi_0$, while the 4-JJ coupling strength goes to zero. We have discussed earlier the benefits of operating qubits near the degeneracy points - where there is a low magnetic field sensitivity to magnetic field variations. The twin qubit allows $|1\rangle \leftrightarrow |2\rangle$ transitions at these optimal working points, while in other flux qubits this transitions are forbidden.

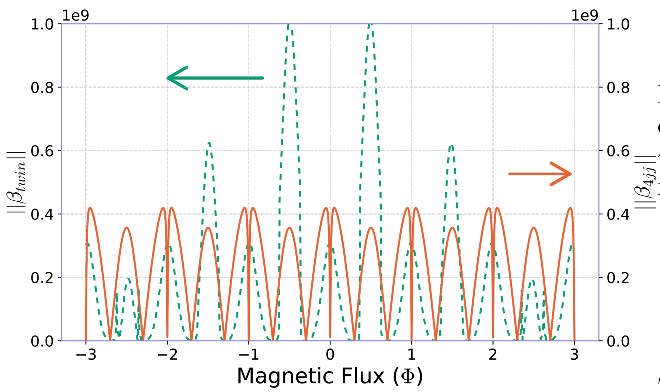


FIG. 5. **Dipole coefficient:** Compared are the absolute magnitudes of $||\beta||$ between the twin qubit (green) and 4-JJ (orange) qubit designs. In simulations we use $E_J = 91\,\mathrm{GHz}, E_C = 13.5\,\mathrm{GHz}, \alpha = 1.023\,, \eta = 1.011$ for the twin qubit and $E_C = 20\,\mathrm{GHz}, E_J = 30\,\mathrm{GHz}, \alpha = 0.45$ for the 4-JJ qubit. The 4-JJ qubit has $|\beta| = 0$ in the vicinity of degeneracy points $\Phi = (n+\frac{1}{2})\Phi_0$, where the transition $|1\rangle \leftrightarrow |2\rangle$ is therefore forbidden.

## V. CONCLUSION

We have fabricated and characterized the first isolated twin qubit. It has weak flux sensitivity and allows $|1\rangle \leftrightarrow |2\rangle$ transitions at degeneracy points $\Phi = n\Phi_0, n \in \mathbb{Z}$. The latter effect is different from other flux based qubits, in which this transition is forbidden. We did not get the high decoherence times, $\tau_{\mathrm{dec}}$ is only 42 ns, but it can be substantially improved by implementation of advanced fabrication techniques the twin qubit may be in competition of serving as the building block of quantum electronic circuits.

# Appendices

## A. DECOHERENCE RESULTS IN LOSS OF QUANTUM INFORMATION

Quantum processing involves manipulating the state of a qubit, $\Psi$, changing the relative state population, $|\alpha| \leq 1$, and phase, $\varphi$, between states $|0\rangle$ and $|1\rangle$:

$$\Psi = \alpha\,|0\rangle + e^{i\varphi}(1-\alpha)\,|1\rangle\,.$$

When written as a density matrix, the phase information is mapped onto the off-diagonal elements:

$$\rho = |\Psi\rangle\langle\Psi| = \begin{pmatrix} |\alpha|^2 & \alpha(1-\alpha)e^{-i\varphi} \\ \alpha(1-\alpha)e^{+i\varphi} & |(1-\alpha)|^2\,. \end{pmatrix}$$

Decoherence, by definition, causes the off-diagonal elements decay to 1/e of the initial value over a time $\tau_{\mathrm{dec}}$. Decoherence causes the loss of computational information encoded in the phase $\varphi$.

## B. REPRESENTATION OF HAMILTONIAN IN THE CHARGE BASIS

The Hamiltonian

$$\begin{aligned}\mathcal{H} &= T + U \\ &= E_C\,|C|\left\langle \hat{C}^{-1}\right\rangle_{|n_1,n_2,n_3\rangle} \\ &\quad + E_J\big[4 + \alpha - \alpha\cos(\varphi_2) - \cos(\varphi_1) - \cos(\varphi_3) - \\ &\qquad \cos(\varphi_2 - \varphi_1 - \varphi_{\mathrm{ext}}) - \cos(\varphi_2 - \varphi_3 + \eta\varphi_{\mathrm{ext}})\big]\end{aligned}$$

in the charge basis takes the form shown in Fig. 6. A state $|-1,0,1\rangle$ would correspond to a CP-occupation of -1, 0 and 1 on islands 1, 2 and 3. In the matrix shown each island can have an occupation $-1 \leq n_i \leq 1$ (3 CP states), for a total of 27 system states. In the simulation, this was increased to 343 by using $-3 \leq n_i \leq 3$ - UNCLEAR WHY THIS VALUE IN PARTICULAR.

Kinetic terms ($T$) naturally fall on the diagonal axis of the matrix. Potential terms ($U$) are expanded to complex exponentials, which become off diagonal elements (see Appendix C).

## C. EXPANSION OF POTENTIAL TERM, $U$, IN THE CP-BASIS

Switching to the CP-basis, leads to a non-trivial representation of phase-dependent terms in

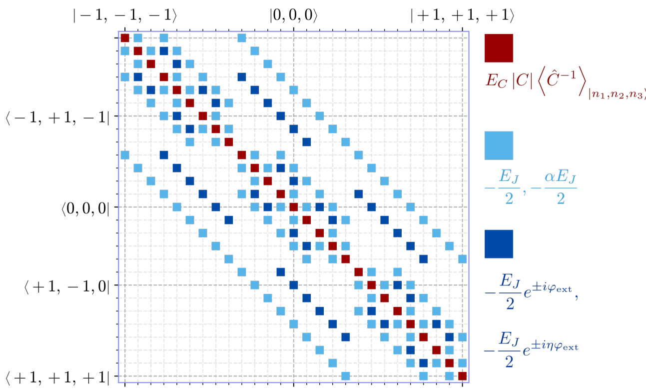


FIG. 6. **Hamiltonian in the CP-basis representation:** Purple square denote the kinetic terms that all fall on the main diagonal. Light blue squares denote simple off-diagonal terms distributed symmetrically about the main diagonal, arising from e.g. $\cos(\varphi_2)$. Dark blue squares are have an additional flux dependence $e^{i\varphi_{\rm ext}}, e^{i\eta\varphi_{\rm ext}}$, arising from e.g. $\cos(\varphi_2-\varphi_1-\varphi_{\rm ext})$.

$U(\varphi_1,\varphi_2,\varphi_3,\varphi_{\rm ext})$. The following explanation will illustrate the expansion process.

1. Derive the commutation relation between the number, $\hat{n}$, and the exponential phase, $e^{\pm i\hat{\varphi}}$, by using the standard relation $[\hat{n},\hat{\varphi}]=1$:

$$\left[\hat{n}, e^{\pm i\hat{\varphi}}\right] = \left[\hat{n}, \sum_{\alpha=0}^{\infty}\frac{(\pm i\hat{\varphi})^{\alpha}}{\alpha!}\right] = \sum_{\alpha=0}^{\infty}(\pm i)^{\alpha}\frac{[\hat{n},\hat{\varphi}^{\alpha}]}{\alpha!}$$
$$= \sum_{\alpha=0}^{\infty}(\pm i)^{\alpha}\frac{-\alpha i\hat{\varphi}^{\alpha-1}}{\alpha!} = \pm\sum_{\alpha=1}^{\infty} i^{\alpha-1}\frac{(\pm\hat{\varphi})^{\alpha-1}}{(\alpha-1)!} = \pm e^{\pm i\hat{\varphi}}.$$

2. Operating with the number operator on state $e^{\pm i\hat{\varphi}}|n\rangle$ and using the commutation result

$$\hat{n}\left[e^{\pm i\hat{\varphi}}|n\rangle\right] = \left[\pm e^{\pm i\hat{\varphi}} + e^{\pm i\hat{\varphi}}\hat{n}\right]|n\rangle$$
$$= (n\pm 1)\left[e^{\pm i\hat{\varphi}}|n\rangle\right].$$

3. Evidently, the exponential phase operator is a ladder operator for the $|n\rangle$ state:

$$e^{\pm i\hat{\varphi}}|n\rangle = |n\pm 1\rangle \Rightarrow e^{\pm i\varphi} = \sum_{n}|n\pm 1\rangle\langle n|\,.$$

4. Thus operator $\cos(\hat{\varphi}_2-\hat{\varphi}_1-\hat{\varphi}_{\rm ext})$ can be expressed in the number basis $\{n_1,n_2,n_3\}$ as:

$$\begin{aligned}
\cos(\hat{\varphi}_2-&\hat{\varphi}_1-\hat{\varphi}_{\rm ext}) = \\
&= \frac{1}{2}\left(e^{i\hat{\varphi}_2}e^{-i\hat{\varphi}_1}e^{-i\hat{\varphi}_{\rm ext}} + \text{c.c.}\right)\\
&= \frac{1}{2}\left(\left[\sum_{n_2}|n_2+1\rangle\langle n_2|\right]\right.\\
&\qquad \left.\otimes\left[\sum_{n_1}|n_1-1\rangle\langle n_1|\right]\otimes\mathbb{I}^{(3)}\right)e^{-i\varphi_{\rm ext}} + \text{c.c.}\\
&= \frac{1}{2}e^{-i\varphi_{\rm ext}}\sum_{n_{1,2,3}}|n_1-1,n_2+1,n_3\rangle\langle n_1,n_2,n_3| + \text{c.c.}
\end{aligned}$$

5. Physically this corresponds to a CP exchange between island 1 and island 2. An example of a term could be

$$\frac{1}{2}e^{-i\varphi_{\rm ext}}|-1,1,0\rangle\langle 0,0,0| + \frac{1}{2}e^{+i\varphi_{\rm ext}}|0,0,0\rangle\langle -1,1,0|\,,$$

which would be a pair of symmetrical off-diagonal elements in the matrix of Fig. 6.

[1] O. Astafiev and A. M. Zagoskin and A. A. Abdumalikov and Yu. A. Pashkin and T. Yamamoto and K. Inomata and Y. Nakamura and J. S. Tsai, Science, **327**, 5967 (2010)

[2] Hoi, Io-Chun and Wilson, C. M. and Johansson, Göran and Palomaki, Tauno and Peropadre, Borja and Delsing, Per, Phys. Rev. Lett., **107**, 073601 (2011)

[3] Hönigl-Decrinis T., Antonov I. V., Shaikhaidarov, R. and Antonov, V. N. and Dmitriev, A. Yu. and Astafiev, O. V., Phys. Rev. A, **98**, 041801 (2018)

[4] Shen, Jung-Tsung and Fan, Shanhui, Phys. Rev. Lett, **95**, 213001 (2005)

[5] M. W. Johnson and P. Bunyk and F. Maibaum and E. Tolkacheva and A. J. Berkley and E. M. Chapple and R. Harris and J. Johansson and T. Lanting and I. Perminov and E. Ladizinsky and T. Oh and G. Rose, Supercond. Sci. Technol., **23**, 065004 (2010)

[6] Linke, Norbert M. and Maslov, Dmitri and Roetteler, Martin and Debnath, Shantanu and Figgatt, Caroline and Landsman, Kevin A. and Wright, Kenneth and Monroe, Christopher, Proceedings of the National Academy of Sciences, **114**, 3305-3310 (2017)

[7] Monroe, C. and Meekhof, D. M. and King, B. E. and Itano, W. M. and Wineland, D. J., Physical Review Letters,**75**, 4714 (1995)

[8] T.P. Orlando and J.E. Mooji and Lin Tian and Caspar H. van der Wal and L. Levitov and Seth Lloyd and J.J. Mazo, Science,**285**, 1036 (1999)

[9] , M. H. Devoret and A. Wallraff and J. M. Martinis (2008)

[10] I. Chiorescu and Y. Nakamura and C. J. P. M. Harmans and J. E. Mooij, Science, **299**, 1869 (2003)

[11] Mooij, J. E. and Orlando, T. P. and Levitov, L. and Tian, Lin and van der Wal, Caspar H. and Lloyd, Seth, Science, 285, **5430** (1999)

[12] A. Cottet, D. Vion, A. Aassime, P. Joyez, D. Esteve, M.H. Devoret, Physica C: Superconductivity, **367**, 197 (2002)

[13] Gu, Xiu and Kockum, Anton Frisk and Miranowicz, Adam and Liu, Yu-xi and Nori, Franco, Physics Reports, **718-719**, 1–102 (2017)

[14] Stern, M. and Catelani, G. and Kubo, Y. and Grezes, C. and Bienfait, A. and Vion, D. and Esteve, D. and Bertet, P., Phys. Rev. Lett.,**113**, 123601 (2014)

[15] Yan, Fei and Gustavsson, Simon and Kamal, Archana and Birenbaum, Jeffrey and Sears, Adam P and Hover, David and Gudmundsen, Ted J. and Rosenberg, Danna and Samach, Gabriel and Weber, S and Yoder, Jonilyn L. and Orlando, Terry P. and Clarke, John and Kerman, Andrew J. and Oliver, William D, Nature Communications, **7**, 12964 (2016)

[16] Yueyin Qiu and Wei Xiong and Xiao-Ling He and Tie-Fu Li and J. Q. You, Scientific Reports, **6**, 28622 (2016)

[17] Pop, Ioan M. and Geerlings, Kurtis and Catelani, Gianluigi and Schoelkopf, Robert J. and Glazman, Leonid I. and Devoret, Michel H., Nature, 508, **369** (2014)

[18] Original bad-ass paper

[19] Yu-Lin Wu and Hui Deng and Hai-Feng Yu and Guang-Ming Xue and Ye Tian and Jie Li and Ying-Fei Chen and Shi-Ping Zhao and Dong-Ning Zheng, Chinese Physics B, 22, 060309 (2013)

[20] C T Earnest et al 2018 Supercond. Sci. Technol. 31 125013

[21] Barends,R. and Wenner,J. and Lenander,M. and Chen,Y. and Bialczak,R. C. and Kelly,J. and Lucero,E. and O'Malley,P. and Mariantoni,M. and Sank,D. and Wang,H. and White,T. C. and Yin,Y. and Zhao,J. and Cleland,A. N. and Martinis,John M. and Baselmans,J. J. A., Applied Physics Letters, 99, 113507, 2011

[22] Abdumalikov, A. A. and Astafiev, O. and Zagoskin, A. M. and Pashkin, Yu. A. and Nakamura, Y. and Tsai, J. S., Phys. Rev. Lett.,104, 193601 (2010)

[23] Zhu,Xiaobo and Kemp,Alexander and Saito,Shiro and Semba,Kouichi, Applied Physics Letters, 97, **102503** (2010)

[24] Gustavsson, S. and Bylander, J. and Yan, F. and Forn-Díaz, P. and Bolkhovsky, V. and Braje, D. and Fitch, G. and Harrabi, K. and Lennon, D. and Miloshi, J. and Murphy, P. and Slattery, R. and Spector, S. and Turek, B. and Weir, T. and Welander, P. B. and Yoshihara, F. and Cory, D. G. and Nakamura, Y. and Orlando, T. P. and Oliver, W. D., Phys. Rev. Lett., **108**, 170503(2012)

[25] Jonas Bylander, Simon Gustavsson, Fei Yan, Fumiki Yoshihara, Khalil Harrabi, George Fitch, David G. Cory, Yasunobu Nakamura, Jaw-Shen Tsai, and William D. Oliver. Noise spectroscopy through dynamical decoupling with a superconducting flux qubit. *Nature Physics*, 7(7):565–570, may 2011.

[26] G. Ithier, E. Collin, P. Joyez, P. J. Meeson, D. Vion, D. Esteve, F. Chiarello, A. Shnirman, Y. Makhlin, J. Schriefl, and G. Schön. Decoherence in a superconducting quantum bit circuit. *Physical Review B*, 72(13), oct 2005.

[27] John M. Martinis, S. Nam, J. Aumentado, K. M. Lang, and C. Urbina. Decoherence of a superconducting qubit due to bias noise. *Physical Review B*, 67(9), mar 2003.